

General Relativistic Decompression of Binary Neutron Stars During Inspiral

Mark Miller

Jet Propulsion Laboratory, California Institute of Technology, Pasadena, California 91109, USA

(Dated: May 24, 2019)

We investigate the dynamic stability of inspiraling neutron stars by performing multiple-orbit numerical relativity simulations of the binary neutron star inspiral process. We find that as the separation between the stars decreases during the inspiral induced by gravitational wave emission, the central rest mass density of each star *decreases*, thus stabilizing each star against collapse. We compare the amount of decompression observed in our numerical relativity simulations with the amount predicted by post-Newtonian approximations.

PACS numbers: 04.25.Dm, 04.30.Db, 04.40.Dg, 02.60.Cb

INTRODUCTION

Detailed and accurate models of binary neutron star coalescence phenomena, from quasi-equilibrium orbits through plunge and merger to the subsequent formation of the final compact object, will be required in order to extract information regarding the structure of neutron stars from detected gravitational wave signals. One detail of some debate over the past decade has been the so-called “neutron star crushing effect”, reported in [1, 2, 3]. This effect was first reported in [1], where binary neutron star simulations employing a variety of simplifying assumptions indicated that as the binary stars spiraled inwards, the general relativistic gravitational interaction between the two stars caused a destabilization, triggering the collapse of each star to individual black holes well *before* the plunge and merger phase of the inspiral. Since then, studies using several different sets of approximations [4, 5, 6, 7, 8, 9, 10] predict the exact opposite, namely that the gravitational interaction between the two stars act to stabilize each star as the binary separation decreases during inspiral. An error in the formulation used in the original “neutron star crushing effect” studies was pointed out in [11]. However, subsequent studies still claim a small destabilization effect [3].

In this Letter, we report on the first fully dynamical general relativistic simulation results aimed at studying this “neutron star crushing effect” for inspiraling binary neutron stars. In the past several years, fully general multiple-orbit binary neutron star simulations have been performed in numerical relativity [12, 13] and their accuracy analyzed [14]. We use the evolution code previously described in [12] to perform multiple-orbit simulations of binary neutron stars. We begin each simulation with initial data corresponding to quasi-equilibrium, circular orbit configurations modified such that the initial orbital angular velocity of the neutron stars is decreased by varying amounts. Each initial data configuration satisfies the initial value constraints of general relativity. The simulations resulting from these eccentric-orbit initial data sets permit the study of the compression/decompression effect by correlating the central rest mass density of the

neutron stars with the proper separation of the stars as the evolution progresses through several apastron (maximum separation) / periastron (minimum separation) points during the inspiral. We find that the stars do, in fact, stabilize as the binary separation decreases. Fitting a power law to the fractional change in central rest mass density ρ_c as a function of the proper separation r_p of the neutron stars

$$\frac{\delta\rho_c}{\rho_c} = F_0 \left(\frac{m}{r_p} \right)^\sigma, \quad (1)$$

we find

$$\sigma = 1.4 \quad F_0 = -0.68 < 0 \quad (2)$$

where m is a measure of the ADM mass of the system. We expect the value of F_0 to be dependent on the equation of state (for our simulations, we use a polytropic equation of state with adiabatic index $\Gamma = 2$), but the fact that we find a negative value for F_0 indicates the stabilizing nature of the binary interaction: as the neutron stars approach each other, the central rest mass density of each star *decreases*, thus stabilizing each star against collapse.

SIMULATION RESULTS

The numerical relativity / general relativistic hydrodynamics code used here is described in [12] and analyzed for accuracy in [14]. The grid size used for all simulations reported here is $643 \times 643 \times 325$, employing a mirror symmetry about the equatorial plane of the neutron stars, $z = 0$. We choose units such that the gravitational constant G and the speed of light c are identically 1. A spatial discretization of $\Delta x/m = 0.148$ is used, which corresponds to roughly 40 points across the diameter of each neutron star. The boundary of the domain is thus eight neutron star diameters away from the center of mass of the system. The physical parameters of three simulations NS-1, NS-2, and NS-3 are shown in Table I. The initial data corresponds to the quasi-equilibrium, circular orbit

Config.	$m\Omega_0$	J_0/m^2	M_0/m	$(\rho_c)_\infty m^2$	$(r_p)_0/m$
NS-1	0.01618	1.121	1.073	0.009076	18.10
NS-2	0.01599	1.094	1.073	0.009010	18.12
NS-3	0.01580	1.067	1.073	0.008947	18.14

TABLE I: The physical parameters of the initial data used for numerical relativity simulations NS-1, NS-2, and NS-3. These initial data sets correspond to quasi-equilibrium, circular orbit initial data with the initial angular velocity Ω_0 reduced from the circular orbit value by 1%, 2%, and 3%, respectively. The symbols J_0 and M_0 are used to denote the initial angular momentum and total rest mass of the configuration, respectively. The central rest mass density of a stationary neutron star configuration in isolation, uniformly rotating with angular velocity Ω_0 is denoted as $(\rho_c)_\infty$, and the initial proper separation of the neutron stars, defined by Eq. 57 in [12], is denoted as $(r_p)_0$. A polytropic equation of state with adiabatic index $\Gamma = 2$ is used. The rest mass of each neutron star corresponds to 82% of the maximum stable TOV rest mass configuration. All physical quantities in this Letter are expressed in units of m , which we define to be twice the ADM mass of a single stationary neutron star configuration with rest mass $M_0/2$ uniformly rotating with angular velocity Ω_0 .

initial data described in [12], except that here, the initial orbital angular velocity parameter Ω_0 has been decreased from the circular orbit value by a factor of 1%, 2%, and 3% for simulation NS-1, NS-2, and NS-3, respectively. The resulting initial data satisfies the Einstein equation initial value constraints, and results in binary evolutions whose orbits contain increasing amounts of eccentricity.

In Fig. 1, the angular momentum of the system J is plotted as a function of coordinate time; $t_{\text{coord}} = 500 m$ corresponds to roughly two orbital periods. For comparison, the angular momentum for solutions to the 2.5 post-Newtonian (dotted curves) and 4.5 post-Newtonian (dashed curves) point particle equations of motion is plotted along side the simulation results (solid curves). The overall rate of decrease in angular momentum for the numerical relativity simulations is roughly equivalent, if not slightly more, than predicted by the post-Newtonian equations of motion. However, the difference in total angular momentum between the numerical relativity simulations NS-1, NS-2, and NS-3 (solid curves) is nearly twice as large as the difference between the post-Newtonian curves, even though the post-Newtonian initial data is selected using the same method as in the numerical relativity case, namely, using circular orbit initial data with a decrease in initial angular velocity of 1%, 2%, and 3% (see Table I). This is most likely due to the nonlinear effects of resolving the constraints of general relativity after decreasing the initial angular velocity parameter Ω_0 when preparing the initial data for the numerical relativity simulations.

In Fig. 2, the coordinate separation is plotted as a function of coordinate time for the numerical relativity

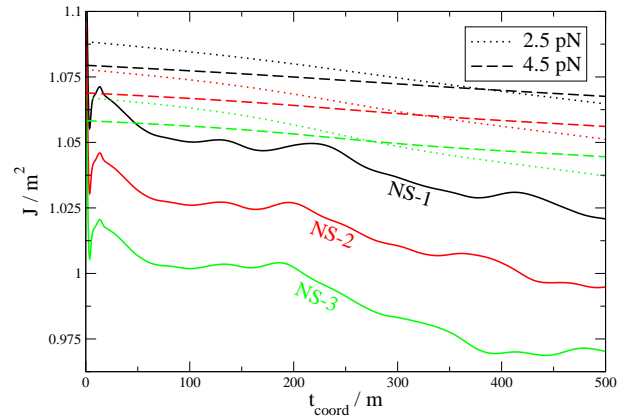


FIG. 1: The total angular momentum J is plotted for the binary neutron star numerical relativity simulations NS-1, NS-2, and NS-3 (solid curves). All simulations correspond to roughly two orbital periods. For comparison, solutions to the post-Newtonian point particle equations of motion are shown, using the same initial coordinate separation, mass, and initial orbital angular velocity (i.e., 1%, 2%, and 3% below the circular orbit angular velocity) as the numerical relativity simulations. Dotted curves are solutions to the 2.5 post-Newtonian (quadrupole level) equations of motion (see, e.g., [15]). Dashed curves are solutions to the 4.5 post-Newtonian equations of motion, which include 3.5 pN [15] and 4.5 pN [16] radiation reaction terms, along with the 3.0 pN [17] conservative terms.

simulations NS-1 (thick solid curve), NS-2 (thick dotted curve), and NS-3 (thick dashed curve). For comparison, solutions to the 4.5 post-Newtonian equations of motion are shown as corresponding thin curves. Contour plots of the rest mass density for the initial data, as well as the first periastron points of simulations NS-1, NS-2, and NS-3, are shown in Fig. 3. The first periastron points occur just slightly before the completion of three-quarters of an orbit for all three simulations.

DECOMPRESSION OF BINARY NEUTRON STARS

In Fig. 4, we plot the proper binary separation r_p (defined to be the spatial geodesic distance between the maximum rest mass density point of each neutron star, see Eq. 57 in [12]) as a function of the proper time t_p measured by observers located at the maximum rest mass density points of the neutron stars. An evolved proper time of $t_p = 300 m$ corresponds to roughly two orbital periods. Also in Fig. 4 is a plot of the maximum rest mass density ρ_{max} of the neutron stars as a function of proper time t_p . Oscillations in $\rho_{\text{max}}(t_p)$ corresponding to the fundamental radial oscillation mode of each neutron star have been filtered out. The proper time period of these oscillations as measured by observers at the maximum rest mass density points of the neutron stars is

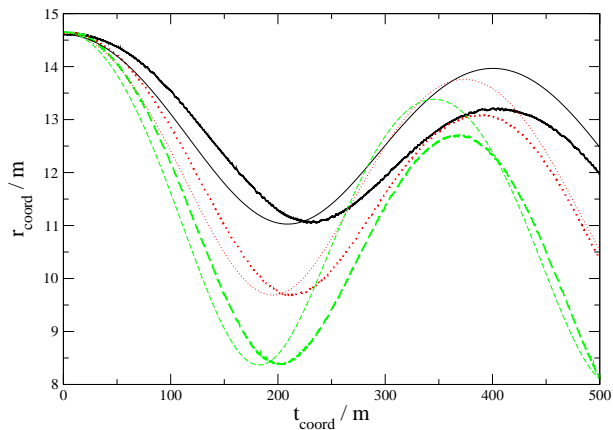


FIG. 2: The coordinate separation of the neutron star binary r_{coord} is plotted as a function of coordinate time t_{coord} for simulations NS-1 (thick solid curve), NS-2 (thick dotted curve), and NS-3 (thick dashed curve). One orbital period corresponds to $\Delta t_{\text{coord}} \approx 250 m$. For comparison, solutions to the 4.5 post-Newtonian equations of motion are shown as corresponding thin curves. The mass and initial separation for the post-Newtonian solutions were chosen to match the numerical relativity initial data, but the initial angular velocity was chosen to match the respective numerical relativity simulation's first periastron coordinate separation. This matching required a reduction in the initial post-Newtonian angular velocity of 10%, 7.3%, and 4.9%, respectively, from the circular orbit angular velocity.

$T_p = 35.0 m$, which is roughly five times smaller than the proper time orbital period and seven times smaller than the proper time observed between apastron (local maximum in separation) points. Fig. 4 displays a clear correlation between the maximum rest mass density of the stars and the proper separation of the stars; smaller proper separation r_p corresponds to smaller maximum rest mass density ρ_{max} . Not only is this correlation evident when comparing apastron/periastron points, but it also exists over gravitational radiation reaction timescales. This is evidenced by comparing both the proper separation of the binary and the maximum rest mass density at successive apastron (local maximum in separation) points in Fig. 4. First, we see that the proper separation r_p at the second apastron point (which occurs at roughly $t_p = 250 m$ for all three simulations) is approximately 10% smaller than the proper separation at the first apastron point (which occurs at the initial time $t_p = 0$). Gravitational radiation emission is draining the binding energy of the binary, causing an overall decrease in separation. We also see from Fig. 4 that the maximum rest mass density of the neutron stars is smaller at the second apastron point as compared to the first apastron point. This is the first demonstration of the stabilizing effect of the general relativistic gravitational interaction between very compact stars in a fully dynamical numerical relativity simulation.

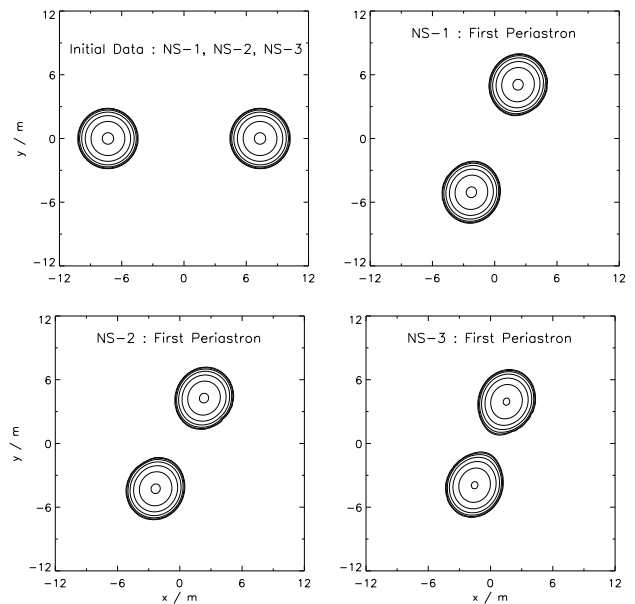


FIG. 3: Contour plots of the rest mass density ρ in the $x-y$ equatorial plane of the binary neutron stars is shown for initial data (upper left) and the first periastron point for simulations NS-1 (upper right), NS-2 (lower left), and NS-3 (lower right). The central contour corresponds to a value of $\rho = 0.0083/m^2$. Six more contours are shown; each successive contour corresponds to a decrease in rest mass density by a factor of two.

Finally, we compare the decompression effect observed in our numerical relativity simulations NS-1, NS-2, and NS-3, with that predicted by a post-Newtonian analysis. In [8], a post-Newtonian matched asymptotic expansion technique is used to obtain an expression for the fractional change in the central density of inspiraling binary neutron stars, perturbative in powers of the “tidal expansion parameter” $\alpha \equiv R/r$ where R is the stellar radius and r is the binary separation, such that

$$\frac{\delta \rho_c}{\rho_c} \propto \alpha^6 \quad (3)$$

as $\alpha \rightarrow 0$. This analysis would lead us to expect a power law Eq. 1 with power parameter $\sigma \approx 6$, since the fractional change in stellar radius R (as measured by computing the proper volume V_p of each neutron star during the simulation and calculating the proper stellar radius R_p according to $R_p = (3V_p/(4\pi))^{1/3}$) is two orders of magnitude smaller than the fractional change in binary separation in our simulations NS-1, NS-2, and NS-3.

We fit the power law Eq. 1 to the numerical relativity simulation data from Fig. 4 by defining

$$\frac{\delta \rho_c}{\rho_c} \equiv \frac{\rho_{\text{max}} - (\rho_c)_\infty}{(\rho_c)_\infty} \quad (4)$$

where $(\rho_c)_\infty$ is the central rest mass density of a stationary neutron star configuration in isolation with a uniformly rotating angular velocity Ω_0 (see Table I). We

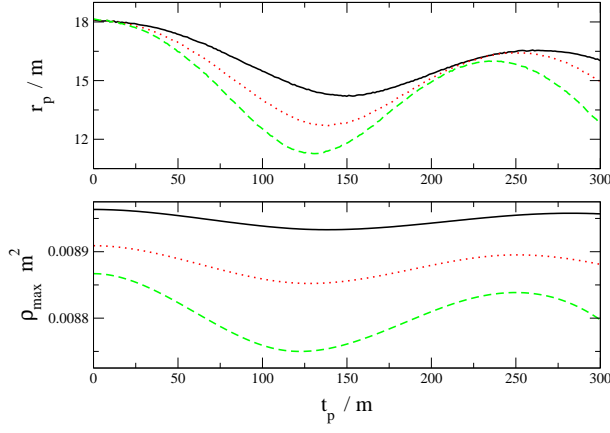


FIG. 4: Top panel: the proper separation of the binary r_p is plotted as a function of proper time t_p as measured by observers at the maximum rest mass density ρ_{\max} of the neutron stars, for numerical relativity simulations NS-1 (solid curve), NS-2 (dotted curve), and NS-3 (dashed curve). Bottom panel: the maximum rest mass density ρ_{\max} of the neutron stars is plotted as a function of t_p for numerical relativity simulations NS-1 (solid curve), NS-2 (dotted curve), and NS-3 (dashed curve). Oscillations in $\rho_{\max}(t_p)$ corresponding to the fundamental radial oscillation mode of each neutron star have been filtered out.

define the function $f(F_0, \sigma)$ to be the square root of the dimensionless average squared error between the power law given by Eqs. 1 and 4, and the numerical relativity simulation data $\{\rho_{\max}(t_p), r_p(t_p)\}$ from Fig. 4 as

$$f(F_0, \sigma) \equiv \sqrt{\frac{\sum_{NS=1}^{NS=3} m^4 \int_0^{300 m} \left[\rho_{\max} - (\rho_c)_\infty \left(1 + F_0 \left(\frac{m}{r_p} \right)^\sigma \right) \right]^2 dt_p}{\sum_{NS=1}^{NS=3} \int_0^{300 m} dt_p}} \quad (5)$$

A global minimum of $f(F_0, \sigma)$ is found at $f(F_0 = -0.68, \sigma = 1.4) = 9.8 \times 10^{-6}$. Finding a negative value for F_0 is in perfect keeping with the correlation between r_p and ρ_{\max} visible in Fig. 4; the actual value $F_0 = -0.68$ is dependent on the equation of state. The result $\sigma = 1.4$ is slightly unexpected, in view of the calculations from [8], Eq. 3, which predicts $\sigma \approx 6$. The cause of this discrepancy is not clear at this time. It may be that the higher order terms (e.g., $\alpha^7, \alpha^8, \dots$) truncated from Eq. 3 need to be taken into account, due to the relatively large values of α used in our simulations (the range of $\alpha = R_p/r_p$ in simulations NS-1, NS-2, and NS-3 is $\alpha = [0.26, 0.42]$). Numerical relativity simulations involving larger relative orbital separations (smaller values of α) will be able to determine the leading order power σ more accurately. It

will take additional computational infrastructure, such as adaptive mesh refinement or higher order accurate methods (possibly both [14]), to carry out such dynamical numerical relativity simulations with an accuracy sufficient to make this determination.

ACKNOWLEDGMENT

It is a pleasure to thank my colleagues at the Jet Propulsion Laboratory for many useful discussions and suggestions. Financial support for this research has been provided by the Jet Propulsion Laboratory under contract with the National Aeronautics and Space Administration. Computational resource support has been provided by the JPL Institutional Computing and Information Services, the NASA Directorates of Aeronautics Research, Science, Exploration Systems, and Space Operations, and NSF NRAC project MCA02N022.

-
- [1] J. Wilson and G. Mathews, Phys. Rev. Lett. **75**, 4161 (1995).
 - [2] J. Wilson, G. Mathews, and P. Marronetti, Phys. Rev. D **54**, 1317 (1996); G. Mathews and J. Wilson, Astrophys. J. **482**, 929 (1997); P. Marronetti, G. Mathews, and J. R. Wilson, Phys. Rev. D **58**, 107503 (1998); G. Mathews, P. Marronetti, and J. Wilson, Phys. Rev. D **58**, 043003 (1998).
 - [3] G. Mathews and J. Wilson, Phys. Rev. D **61**, 127304 (2000); J. Wilson, Phys. Rev. D **66**, 084015 (2002); J. Wilson and G. Mathews, Astrophys. J. **610**, 368 (2004); D. S. P. Dearborn, J. Wilson, and G. Mathews, Astrophys. J. **630**, 309 (2005).
 - [4] D. Lai, Phys. Rev. Lett. **76**, 4878 (1996).
 - [5] A. G. Wiseman, Phys. Rev. Lett. **79**, 1189 (1997).
 - [6] P. R. Brady and S. A. Hughes, Phys. Rev. Lett. **79**, 1186 (1997).
 - [7] T. W. Baumgarte, G. B. Cook, M. A. Scheel, S. L. Shapiro, and S. A. Teukolsky, Phys. Rev. Lett. **79**, 1182 (1997).
 - [8] E. E. Flanagan, Phys. Rev. D **58**, 124030 (1998).
 - [9] K. S. Thorne, Phys. Rev. D **58**, 124031 (1998).
 - [10] E.ourgoulhon, P. Grandclément, K. Taniguchi, J. Marck, and S. Bonazzola, Phys. Rev. D **63**, 064029 (2001).
 - [11] E. Flanagan, Phys. Rev. Lett. **82**, 1354 (1999).
 - [12] M. Miller, P. Gressman, and W.-M. Suen, Phys. Rev. D **69**, 64026 (2004).
 - [13] P. Marronetti, M. D. Duez, S. L. Shapiro, and T. W. Baumgarte, Phys. Rev. Lett. **92**, 141101 (2004).
 - [14] M. Miller, Phys. Rev. D **71**, 104016 (2005).
 - [15] M. E. Pati and C. M. Will, Phys. Rev. D **65**, 104008 (2002).
 - [16] A. Gopakumar, B. Iyer, and S. Iyer, Phys. Rev. D **55**, 6030 (1997).
 - [17] L. Blanchet and B. Iyer, Class. Quantum Grav. **20**, 755 (2003).